

# Dye Surface Coating Enables Visible Light Activation of TiO<sub>2</sub> Nanoparticles Leading to Degradation of Neighboring Biological Structures

Jay Blatnik,<sup>1,†</sup> Lanette Luebke,<sup>1,†</sup> Stephanie Simonet,<sup>1</sup> Megan Nelson,<sup>1</sup> Race Price,<sup>1</sup> Rachael Leek,<sup>1</sup> Leyong Zeng,<sup>2</sup> Aiguo Wu,<sup>2</sup> and Eric Brown<sup>1,\*</sup>

<sup>1</sup>Department of Biological Sciences, University of Wisconsin-Whitewater, Whitewater, WI 53190, USA

<sup>2</sup>Division of Functional Materials and Nano Devices, Key Laboratory of Magnetic Materials and Devices,

Ningbo Institute of Materials Technology and Engineering, Chinese Academy of Sciences, Ningbo 315201, China

**Abstract:** Biologically and chemically modified nanoparticles are gaining much attention as a new tool in cancer detection and treatment. Herein, we demonstrate that an alizarin red S (ARS) dye coating on TiO<sub>2</sub> nanoparticles enables visible light activation of the nanoparticles leading to degradation of neighboring biological structures through localized production of reactive oxygen species. Successful coating of nanoparticles with dye is demonstrated through sedimentation, spectrophotometry, and gel electrophoresis techniques. Using gel electrophoresis, we demonstrate that visible light activation of dye-TiO<sub>2</sub> nanoparticles leads to degradation of plasmid DNA *in vitro*. Alterations in integrity and distribution of nuclear membrane associated proteins were detected via fluorescence confocal microscopy in HeLa cells exposed to perinuclear localized ARS-TiO<sub>2</sub> nanoparticles that were photoactivated with visible light. This study expands upon previous studies that indicated dye coatings on TiO<sub>2</sub> nanoparticles can serve to enhance imaging, by clearly showing that dye coatings on TiO<sub>2</sub> nanoparticles can also enhance the photoreactivity of TiO<sub>2</sub> nanoparticles by allowing visible light activation. The findings of our study suggest a therapeutic application of dye-coated TiO<sub>2</sub> nanoparticles in cancer research; however, at the same time they may reveal limitations on the use of dye assisted visualization of TiO<sub>2</sub> nanoparticles in live-cell imaging.

**Key words:** TiO<sub>2</sub>, nanoparticle, alizarin red s (ARS), dye, cancer, reactive oxygen species, membrane proteins, photoactivation

## INTRODUCTION

Titanium dioxide (TiO<sub>2</sub>) nanoparticles are being investigated as a promising new tool for cancer detection and treatment, due to their corner defects that enable surface conjugation of multiple ligands and specific targeting of the nanoparticles (Rajh et al., 2002; Paunesku et al., 2003, 2007, 2008; Brown et al., 2008; Wu, 2008; Thurn et al., 2009, 2011). In this regard, TiO<sub>2</sub> nanoparticles can also be activated when excited with ultraviolet (UV) light in excess of 3.2 eV to produce reactive oxygen species that are capable of inducing damage to neighboring biological agents (Park et al., 2008; Thevenot et al., 2008; Tsuang et al., 2008). However, exposure of biological samples to UV light is less than optimal as this source is a well-documented mutagen. The fluorescent dye, alizarin red S (ARS), has been shown to conjugate successfully to TiO<sub>2</sub> nanoparticles and enhance visualization of these nanoparticles both *in vitro* and *in situ* (Brown et al., 2008; Thurn et al., 2009). At the same time, conjugation of this dye lowers the band gap required for activation of TiO<sub>2</sub> nanoparticles and enhances the production of reactive oxygen species (Liu et al., 2000; Rajh et al., 2002). Consequently, coating TiO<sub>2</sub> nanoparticles with fluorescent dyes such as ARS promises to enable activation of

TiO<sub>2</sub> nanoparticles with a lower intensity visible light source (instead of mutagen-inducing UV light), thus broadening their use in biological applications.

The findings of the current study demonstrate that upon exposure to lower intensity visible light (versus UV light), dye coated-TiO<sub>2</sub> nanoparticles can be activated and degrade neighboring biological structures. We demonstrate that visible light activation of ARS-coated TiO<sub>2</sub> nanoparticles leads to degradation of plasmid DNA *in vitro* as witnessed through changes in plasmid conformation detected via gel electrophoresis. Additionally, through two-dimensional (2D) and three-dimensional (3D) fluorescence confocal microscopy, we show that perinuclear localized ARS-TiO<sub>2</sub> nanoparticles induce DNA condensation in HeLa cells. Visible light activation of these same dye-coated TiO<sub>2</sub> nanoparticles results in enlarged nuclei along with alterations in integrity and distribution of two different nuclear membrane associated proteins (emerin and lamin B1).

The findings presented in this study reveal a therapeutic application of dye-coated TiO<sub>2</sub> nanoparticles in cancer research that does not depend upon mutagen-inducing UV light activation, but rather enables lower intensity, visible light activation. At the same time, the results also suggest limitations on the use of dye assisted visualization of TiO<sub>2</sub> nanoparticles in live-cell imaging due to their enhanced visible light activation and ability to degrade neighboring biological structures.

Received July 8, 2011; accepted September 12, 2011

\*Corresponding author. E-mail: brown@uw.edu

†These authors contributed equally to this work.

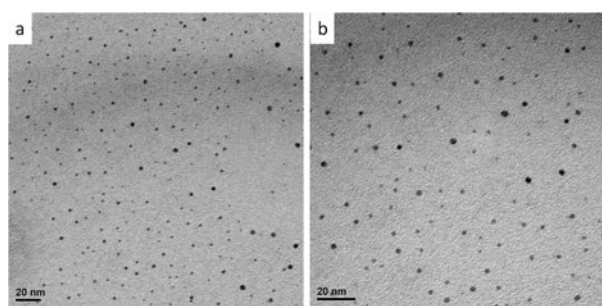


**Figure 1.** TEM images depict the approximately 6 nm  $\text{TiO}_2$  nanoparticles used in the study. Scale bar = 20 nm.

## MATERIALS AND METHODS

### Preparation of Titanium Dioxide Nanoparticles and Characterization by Transmission Electron Microscopy

For the synthesis of 6 nm  $\text{TiO}_2$  nanoparticles,  $\text{TiCl}_4$  was used as the reaction agent, and cetyltrimethyl ammonium bromide (CTAB) was used as the dispersant. All agents were purchased from Guoyao Ltd (China) as analytical pure grade and deionized water was used as solvent. Before the experiment, 0.1 M  $\text{TiCl}_4$  in 20% HCl solution was first prepared and stored at  $-20^\circ\text{C}$ . The synthesis of  $\text{TiO}_2$  nanoparticles was carried out using a magnetic stirrer and the reaction temperature was about  $4^\circ\text{C}$ , which was controlled in an ice bath. First, 10 mL of 0.1 M  $\text{TiCl}_4$  solution was gradually dropped into 200 mL of deionized water under vigorous stirring, and the reaction was maintained for approximately 4 h. Then 10 mL of 0.5 mM CTAB was dropped into the solution, and the solution was continuously stirred magnetically for approximately 1 h. Finally, the product was purified by dialyzing the  $\text{TiO}_2$  colloids in deionized water five times, and the powder of  $\text{TiO}_2$  nanoparticles was prepared by freezing out using a freeze drier. The morphology of  $\text{TiO}_2$  nanoparticles was characterized with a Tecnai F20 (FEI Company, Hillsboro, OR, USA) transmission electron microscope (TEM). The TEM sample was prepared by dropping the  $\text{TiO}_2$  nanoparticles dispersed in water onto a carbon-coated copper grid. Figures 1a and 1b show TEM images of  $\text{TiO}_2$  nanoparticles under different magnifications. It can be seen that the  $\text{TiO}_2$  nanoparticles were well dispersible and of single crystal size of approximately 6 nm.

### Assessing Dye Coating of Nanoparticles

Six nanometer  $\text{TiO}_2$  nanoparticles were synthesized and characterized through the methods described above. The interaction of two dyes, ARS (Sigma, St. Louis, MO, USA) and orange G (Sigma), with  $\text{TiO}_2$  nanoparticles was investigated through four different methods: sedimentation, spectral light absorbance, spectral fluorescence emission, and polyacrylamide gel electrophoresis. Sedimentation assays were performed by incubating each respective dye and  $\text{TiO}_2$  nanoparticles, centrifuging samples at 0.2 g for 3 min, then imaging with a Canon Powershot 7.1 Megapixel A620 digital camera. Shifts in spectral light absorbance and spectral

fluorescence emission between dyes and dye-coated  $\text{TiO}_2$  nanoparticle samples were measured with a NanoDrop 2000 UV-Vis spectrophotometer as described previously (Thurn et al., 2009) and NanoDrop 3300 Fluorospectrometer, respectively (Thermo Fisher Scientific, Waltham, MA, USA). Stability between dye- $\text{TiO}_2$  nanoconjugates was assessed by running samples through a 16% polyacrylamide gel for 2 h as described previously (Brown et al., 2008).

### Effect of Visible and UV Light Photoactivation of Dye- $\text{TiO}_2$ Nanoconjugates on Plasmid DNA

The effect of visible light activated ARS-coated  $\text{TiO}_2$  nanoparticles was assessed by illuminating plasmid containing samples with a Fiber-Lite MI-150 High Intensity Fiber Optic EKE 150 W 21 V Halogen Light Illuminator (Dolan-Jenner Industries, Boxborough, MA, USA) for 10 min. The effect of UV light on activated ARS-coated  $\text{TiO}_2$  nanoparticles was assessed by illuminating plasmid containing samples with a 390 nm 13 W UV light source (Bayco, Wylie, TX, USA). All samples were then run on a 1.25% agarose gel at 60 V for 4 h, stained with GelStar (Lonza, Mapleton, IL, USA), and imaged on a Kodak Gel Logic 2200 Imaging System (Kodak, Rochester, NY, USA).

### Cell Culture, Fixing and Staining, and Confocal Microscopy

HeLa cells were grown on #1 glass coverslips to approximately 20% confluence and then exposed to ARS-coated  $\text{TiO}_2$  nanoparticles or appropriate controls overnight. Respective samples were either exposed to no light or light with a Fiber-Lite MI-150 High Intensity Fiber Optic 150W Halogen Light Illuminator for 10 min. All samples were fixed in 3.6% formaldehyde (Fisher Scientific, Waltham, MA, USA) and permeabilized in 0.2% Triton-100x (Fisher Scientific) for 10 min. Cells were then stained with either a mouse monoclonal to emerin primary antibody (Abcam, Cambridge, MA, USA) followed by an Alexa488 goat anti-mouse IgG (H + L) secondary antibody (Invitrogen, Grand Island, NY, USA) or a chicken polyclonal to lamin B1 primary antibody (Abcam) followed by an Alexa488 goat anti-chicken IgG (H + L) secondary antibody (Invitrogen). All samples were then stained with Hoechst 33342 (Sigma) and coverslips were mounted in P-phenylenediamine containing mounting media. Samples were imaged on an Olympus IX81-UCB Spinning Disc Confocal Microscope (Olympus, Center Valley, PA, USA) using a 100 W mercury burner (Ushio, Tokyo, Japan), Brightline filters for DAPI, FITC, and TEXAS RED (Semrock, Rochester, NY, USA), and an ORCA-ER-1394 high-resolution digital camera (Hamamatsu, Japan). All images are presented as 1  $\mu\text{m}$  optical slice fluorescence overlays in either two or three dimensions.

## RESULTS

### Fluorescent Dye Coating of $\text{TiO}_2$ Nanoparticles

Approximately six nanometer diameter titanium dioxide ( $\text{TiO}_2$ ) nanoparticles were used throughout this investiga-

tion (Figs. 1a, 1b). To demonstrate the successful coating of TiO<sub>2</sub> nanoparticles with the fluorescent dye, ARS, we utilized established techniques such as sedimentation, spectrophotometry, and polyacrylamide gel electrophoresis (Brown et al., 2008; Thurn et al., 2009) and also incorporated an additional assay to measure variations in fluorescence spectral emission of samples. In the sedimentation assay, test tubes containing either (1) dH<sub>2</sub>O, (2) ARS, (3) TiO<sub>2</sub> nanoparticles, or (4) ARS-coated TiO<sub>2</sub> nanoparticles were prepared. Upon centrifugation of these samples at 0.2 g, TiO<sub>2</sub> nanoparticles sedimented out of solution and formed a white pellet on the test tube bottom (Fig. 2a, tube 3), whereas free ARS dye did not sediment under the same conditions (Fig. 2a, tube 2). In the tube containing ARS dye and TiO<sub>2</sub> nanoparticles, a red pellet was observed at the bottom of the test tube, indicating successful conjugation between ARS and TiO<sub>2</sub> nanoparticles (Fig. 2a, tube 4). In contrast, when an alternative dye, orange G, was used under the same conditions as a negative control, the pellet in tube 4 containing dye and TiO<sub>2</sub> nanoparticles remained white and the dye remained in the supernatant, indicating no interaction between orange G and TiO<sub>2</sub> nanoparticles (Fig. 2b). When measuring spectral absorbance, ARS-coated TiO<sub>2</sub> nanoparticles demonstrated a red shift in spectral absorbance compared to their ARS counterparts (Fig. 2c), indicative of a dye-nanoparticle interaction (Thurn et al., 2009). Under the same conditions, no shift in absorbance was witnessed for orange G and TiO<sub>2</sub> counterparts (Fig. 2d). In the gel electrophoresis assay, we utilized the fact that TiO<sub>2</sub> nanoparticles do not enter into a polyacrylamide gel during standard electrophoresis (Paunesku et al., 2003), while selected dyes do enter into such a gel (Brown et al., 2008) to assess dye-TiO<sub>2</sub> nanoparticle interactions. The same samples described above were used. Upon polyacrylamide gel electrophoresis of samples, ARS (Fig. 2e, lane 2) migrated through the gel, while TiO<sub>2</sub> nanoparticles (Fig. 2e, lane 3) and ARS-coated TiO<sub>2</sub> nanoparticles remained trapped in the wells of the gel and a distinct red band was visible (Fig. 2e, lane 4). Under the same conditions, orange G did not remain associated with TiO<sub>2</sub> nanoparticles in the gel well, but rather migrated into the gel (Fig. 2f, lane 4). Thus, in the case of the orange G, both lanes 3 and 4 possessed a white band in the well of the gel. This electrophoresis data further supported the ability of ARS dye to successfully coat TiO<sub>2</sub> nanoparticles, and the remaining experiments within this study utilized ARS-coated TiO<sub>2</sub> nanoparticles. These results supported the findings in the literature that enediol bidentate ligands such as ARS covalently interact with TiO<sub>2</sub> nanoparticles of less than 20 nm in diameter, whereas similar ring structured molecules lacking these functional groups (such as orange G) do not interact (Rajh et al., 2002) (Figs. 3g–3h). ARS and orange G dyes were selected for these reasons. Further support for interaction between ARS and TiO<sub>2</sub> nanoparticles was gained by viewing differences in the fluorescence emissions between ARS and ARS-coated TiO<sub>2</sub> nanoconjugates that were excited by either UV, blue, or visible light. ARS dye was excitable by both blue and

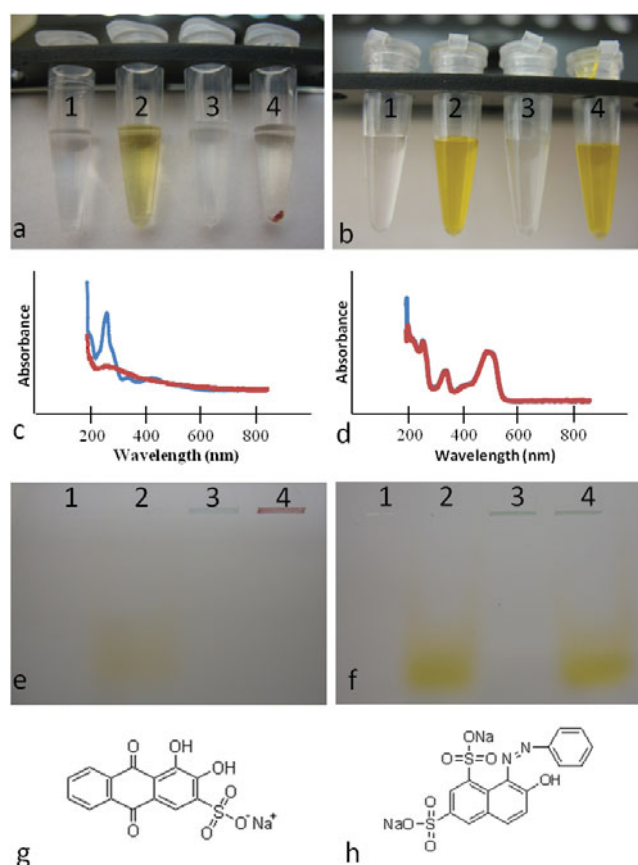


**Figure 2.** The interaction between ARS and TiO<sub>2</sub> nanoparticles and lack of interaction between orange G and TiO<sub>2</sub> nanoparticles is demonstrated through three different assays. **a:** A sedimentation assay illustrated that upon centrifugation of samples at 0.2 g, ARS (tube 2) remained in the supernatant, while TiO<sub>2</sub> nanoparticles (tube 3) and ARS-TiO<sub>2</sub> nanoparticle conjugates (tube 4) formed a pellet at the bottom of the tube (tube 1 = dH<sub>2</sub>O). **b:** Under the same conditions, no orange G-TiO<sub>2</sub> interaction was seen in tube 4 (tube 1 = dH<sub>2</sub>O, tube 2 = orange G, tube 3 = TiO<sub>2</sub> nanoparticles). **c:** ARS-coated TiO<sub>2</sub> nanoparticles (red line) demonstrated a red shift in spectral absorbance compared to their ARS counterparts (blue line). **d:** Under the same conditions, no shift in absorbance was witnessed for orange G-TiO<sub>2</sub> nanoparticles (red line) versus orange G (blue line). **e:** Upon polyacrylamide gel electrophoresis of samples, ARS (lane 2) migrated through the gel, while TiO<sub>2</sub> nanoparticles (lane 3) and dye-TiO<sub>2</sub> nanoparticles (lane 4) remained trapped in the wells of the gel (tube 1 = dH<sub>2</sub>O). **f:** Under the same conditions, orange G did not remain associated with TiO<sub>2</sub> nanoparticles in the gel well, but rather migrated into the gel (lane 4). **g:** Molecular structure of ARS is shown (Sigma). **h:** Molecule structure of orange G is shown (Sigma).

visible light and exhibited an emission maximum between 563–565 nm (Fig. 3a). On the other hand, ARS-coated TiO<sub>2</sub> nanoconjugates were not comparably excited by either UV or blue light and were only excitable by white light, with an emission maximum of 609 nm (Fig. 3b). Compared to ARS, the lack of excitation of ARS nanoconjugates with blue light and the red shift in fluorescence emission when excited with white light is supportive of ARS-TiO<sub>2</sub> interaction. It is also consistent with the red shift in absorbance witnessed

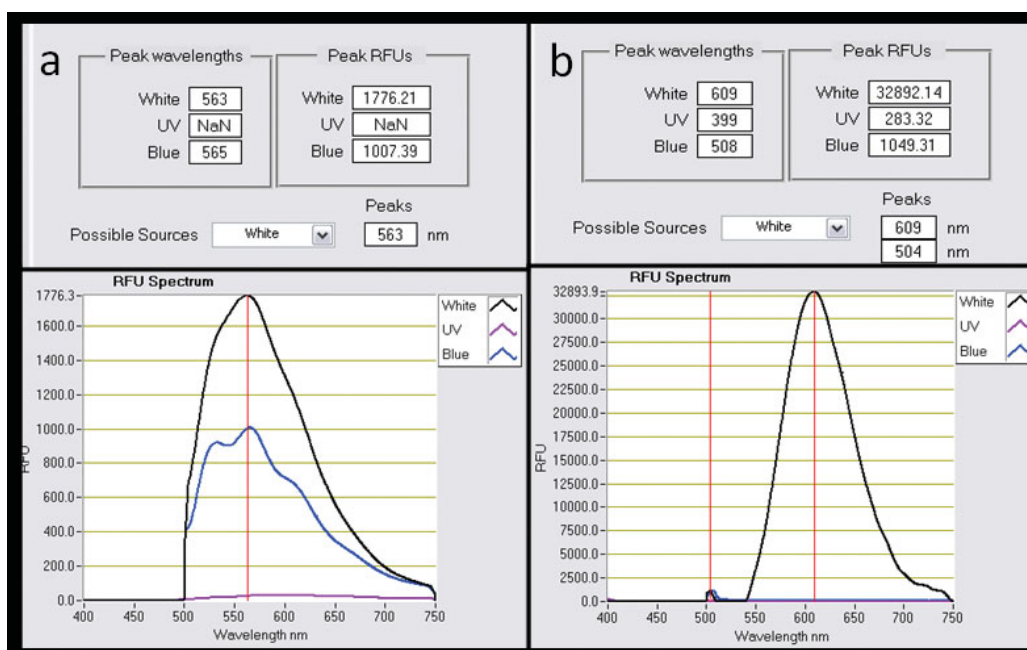


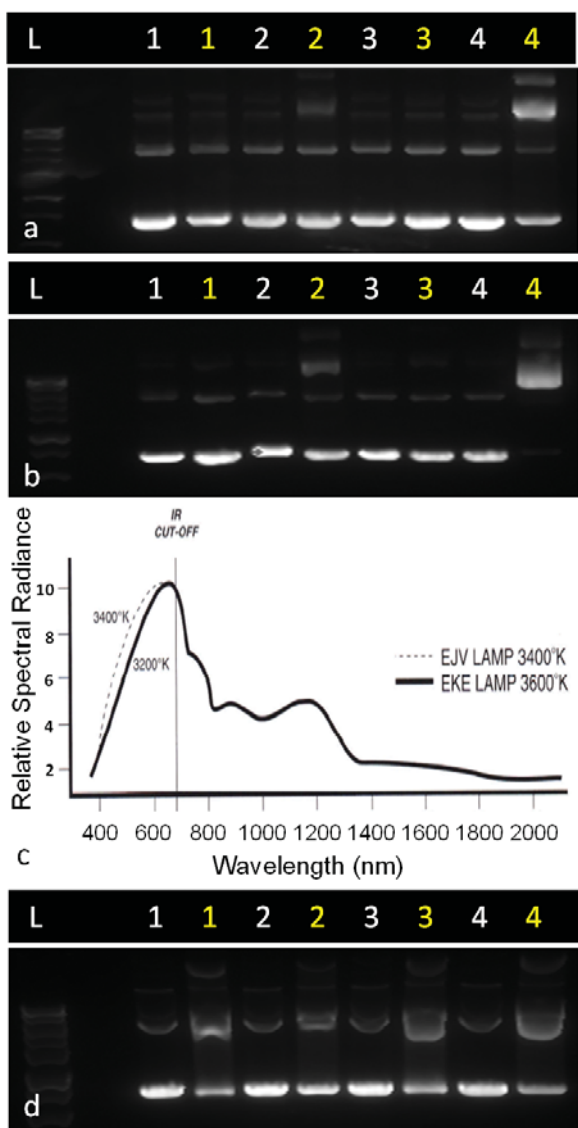
**Figure 3.** Characteristic of dye-TiO<sub>2</sub> interactions, (a) ARS and (b) ARS-coated TiO<sub>2</sub> nanoparticles exhibited different fluorescence emissions when excited by white light.

when comparing ARS with ARS-coated TiO<sub>2</sub> nanoparticles (Figs. 2c, 2d). The fluorescence emission data also proved valuable in the confocal microscopy studies described later.

### Visible Light Activated ARS-Coated TiO<sub>2</sub> Nanoparticles Degrade Plasmid DNA

As stated previously, it has been shown that dyes in general and ARS/TiO<sub>2</sub> dispersions in particular are capable of releasing reactive oxygen species upon photoactivation by visible light (Liu et al., 2000; Sugden, 2004). Additionally, the DNA phosphate backbone has affinity for TiO<sub>2</sub> (Michelmore et al., 2000). Considering these factors, we sought to determine the effect of visible light activated ARS-coated TiO<sub>2</sub> nanoparticles on plasmid DNA integrity using a standard agarose gel electrophoresis technique developed by others. According to this assay, nicked (single-stranded DNA break), linear (double-stranded DNA break), and supercoiled (undamaged) plasmid DNA can be distinguished on an agarose gel by viewing differences in mobility (with the nicked plasmid DNA migrating at the slowest rate and supercoiled plasmid DNA migrating at the fastest rate) (Sugden et al., 2004; Arzac & Hidaka, 2007). Samples were prepared that contained plasmid DNA and either (1) dH<sub>2</sub>O, (2) ARS, (3) TiO<sub>2</sub> nanoparticles, or (4) ARS-coated TiO<sub>2</sub> nanoparticles. Half of each of the four samples was exposed for 10 min to either no light or visible light from an EKE 150W 21V halogen bulb, and all samples were then loaded on a 1.25% agarose gel and electrophoresis was run for 5 h at 50 V (Fig. 4a). All samples contained various configurations of plasmid DNA and the major conformation was supercoiled in form, with the following exception. When plasmid DNA was exposed to visible light activated ARS-coated TiO<sub>2</sub> nanoparticles (Fig. 4a, yellow lane 4), an increase in nicked

(single-stranded break) plasmid DNA was observed accompanied by a respective decrease in supercoiled (undamaged) plasmid DNA. Such an increase in nicked plasmid DNA was not seen in samples containing dark exposed ARS-coated TiO<sub>2</sub> nanoparticles or any other samples, with the exception of a slight expected increase in nicked plasmid DNA in visible light exposed samples containing ARS (Fig. 4a, yellow lane 2). This effect was time dependent as a further increase in nicked plasmid was evident upon exposure to ARS-coated TiO<sub>2</sub> nanoparticles under the same light source for 20 min (Fig. 4b, yellow lane 4). This electrophoresis data demonstrated the ability of ARS-coated TiO<sub>2</sub> nanoparticles to induce strand breakage in DNA upon activation by visible light. The relative spectral radiance for the quartz-halogen bulb used in this study is presented (Fig. 4c). For comparison, the experiment presented in Figure 4a was repeated substituting an UV light source in place of the visible light source. An exposure of UV was selected that resulted in the same level of plasmid nicking achieved previously (compare Fig. 4d, yellow lane 4 versus Fig. 4a, yellow lane 4 and Fig. 4d, yellow lane 2 versus Fig. 4a, yellow lane 2). However, when plasmid samples were exposed to UV light in the presence of bare TiO<sub>2</sub> nanoparticles, a similar level of plasmid nicking was detected (Fig. 4d, yellow lane 3). This was expected because TiO<sub>2</sub> nanoparticles are known to be activated by such UV light sources (Rajh et al., 2002; Gole et al., 2004; Hashimoto et al., 2005). Such activation of bare TiO<sub>2</sub> nanoparticles was not witnessed when samples were exposed to visible light (Fig. 4a, yellow lane 3). Upon exposure to UV light, samples containing solely plasmid DNA exhibited moderate plasmid nicking (Fig. 4d, yellow lane 1) while no such plasmid nicking was detected in solely plasmid samples exposed to visible light (Fig. 4a, yellow lane 1).



### Alterations in Integrity and Distribution of Nuclear Membrane Associated Proteins Resulting from Visible Light Activated ARS-Coated Nanoparticles

Perinuclear localization of ARS-TiO<sub>2</sub> nanoconjugates was previously observed in cancer cells via fluorescence confocal microscopy by comparing nanoconjugate localization to DNA staining within the nucleus and also via X-ray fluorescence microscopy (Thurn et al., 2009, 2011). We expanded upon these studies in our current investigation by viewing the spatial relation of ARS-TiO<sub>2</sub> nanoparticles to two nuclear membrane associated proteins, emerin and lamin B1 (Fig. 5), and determining the effect of visible light activated ARS-coated TiO<sub>2</sub> nanoparticles on the integrity and distribution on these membrane associated proteins via fluorescence confocal microscopy (Figs. 6–8). Perinuclear localization of ARS-coated TiO<sub>2</sub> nanoparticles was evident in viewing a Z-stack series of HeLa cells (1  $\mu$ m optical slices) and comparing the relation of ARS-coated TiO<sub>2</sub> nanoparticles to emerin (green) (Figs. 5a–5l). Localization of ARS-coated TiO<sub>2</sub> nanoparticles is emphasized by white arrows. Furthermore, 3D

**Figure 4. a:** Increased nicking of plasmid DNA was evident when ARS-coated TiO<sub>2</sub> nanoparticles were exposed to visible light for 10 min (lane 4, yellow) compared to no light (lane 4, white), and this increase in nicking was greater than when ARS was exposed to visible light (lane 2, yellow). All lanes contained plasmid DNA + either: lane 1 = no addition, lane 2 = ARS, lane 3 = TiO<sub>2</sub> nanoparticles, lane 4 = ARS-coated TiO<sub>2</sub> nanoparticles, yellow = visible light exposure, white = no light exposure. **b:** Further nicking of plasmid DNA was evident when ARS-coated TiO<sub>2</sub> nanoparticles were exposed to visible light for 20 min and little supercoiled plasmid remained (lane 4, yellow) compared to no light (lane 4, white). The increase in plasmid nicking witnessed in the presence of visible light activated ARS-coated nanoparticles was greater than when ARS was exposed to visible light (lane 2, yellow). All lanes contained plasmid DNA + either: lane 1 = no addition, lane 2 = ARS, lane 3 = TiO<sub>2</sub> nanoparticles, lane 4 = ARS-coated TiO<sub>2</sub> nanoparticles, yellow = visible light exposure, white = no light exposure. **c:** The relative spectral radiance of a quartz-halogen bulb (Dolan-Jenner, modified). **d:** Increased nicking of plasmid DNA was evident when ARS-coated TiO<sub>2</sub> nanoparticles were exposed to UV light for 10 min (lane 4, yellow) compared to no light (lane 4, white). This increase in plasmid nicking was greater than when ARS was exposed to UV light (lane 2, yellow), but approximately the same as when TiO<sub>2</sub> nanoparticles were exposed to UV light (lane 3, yellow). Samples containing solely plasmid DNA that were exposed to UV light did demonstrate detectable levels of plasmid nicking (lane 1, yellow). All lanes contained plasmid DNA + either: lane 1 = no addition, lane 2 = ARS, lane 3 = TiO<sub>2</sub> nanoparticles, lane 4 = ARS-coated TiO<sub>2</sub> nanoparticles, yellow = visible light exposure, white = no light exposure.

reconstructions of 1  $\mu$ m optical slices taken through individual HeLa cells also supported perinuclear localization (Figs. 5m, 5n). In addition to dye-coated nanoparticles exhibiting standard perinuclear localization, some others interacted with HeLa cells in a unique manner, creating a donut effect with emerin tunneling through the center of the HeLa cell and encompassing the ARS-coated TiO<sub>2</sub> nanoparticles (Fig. 5n, central yellow arrow).

Next, we sought to determine the effect of visible light excitation of ARS-coated TiO<sub>2</sub> nanoparticles on emerin integrity and distribution. HeLa cells were exposed to either dH<sub>2</sub>O, ARS, TiO<sub>2</sub> nanoparticles, or ARS-coated TiO<sub>2</sub> nanoparticles and either light or no light conditions (Fig. 6). Large scale alterations in emerin integrity and distribution were detected in HeLa cells exposed to ARS-coated TiO<sub>2</sub> nanoparticles and 150 W halogen white light for 10 min (Fig. 6h), as nuclear rim staining of emerin was decreased and more punctuated (white arrows), compared to HeLa cells exposed to ARS-coated TiO<sub>2</sub> nanoparticles under dark conditions (Fig. 6d). Some DNA condensation was observed in cells exposed to ARS-TiO<sub>2</sub> nanoparticles independent of light exposure (Figs. 6d, 6h), and some enlarged nuclei were also observed when ARS-coated TiO<sub>2</sub> nanoparticles were exposed to visible light. HeLa cells exposed to dH<sub>2</sub>O (Figs. 6a, 6e), ARS (Figs. 6b, 6f), and TiO<sub>2</sub> nanoparticles (Figs. 6c, 6g) exhibited normal emerin integrity and distribution regardless of light treatment. The effect of visible light excitation of ARS-coated TiO<sub>2</sub> nanoparticles on the integrity and

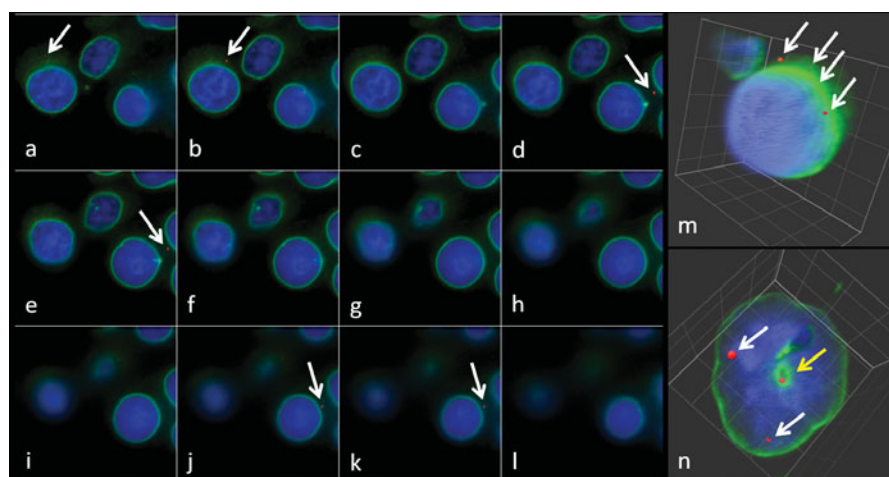


**Figure 5.** **a–l:** Perinuclear localization of ARS-coated TiO<sub>2</sub> nanoparticles was evident in viewing a Z-stack of HeLa cells (1  $\mu$ m optical slices). Localization of ARS-TiO<sub>2</sub> nanoconjugates is indicated by white arrows. **m–n:** Perinuclear localization of ARS-TiO<sub>2</sub> nanoconjugates was also viewed in 3D reconstructions of individual HeLa cells, while some cells also demonstrated membrane encompassing ARS-coated TiO<sub>2</sub> nanoparticles (central yellow arrow in N). Blue = DNA, green = emerin, red = ARS-coated TiO<sub>2</sub> nanoparticles.

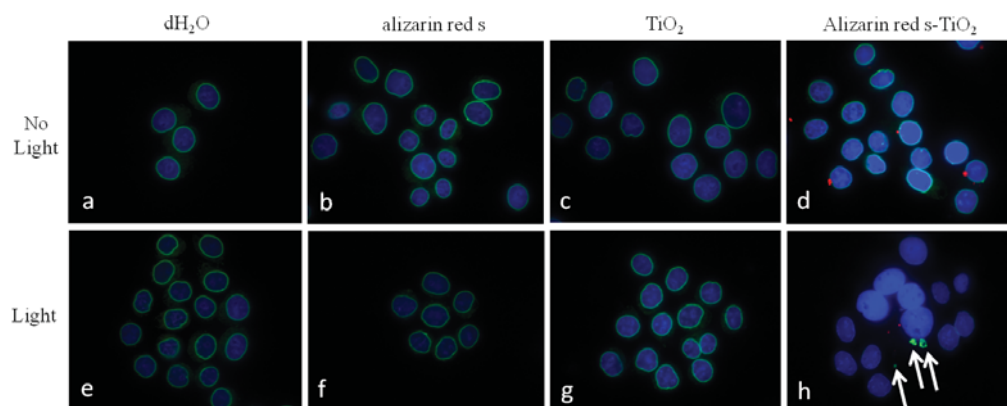


**Figure 6.** Alterations in emerin integrity and distribution were detected in HeLa cells exposed to ARS-coated TiO<sub>2</sub> nanoparticles and 150 W halogen white light for 10 min (**h**), as nuclear rim staining was decreased and more punctuated (white arrows), compared HeLa cells exposed to ARS-coated TiO<sub>2</sub> nanoparticles, but no white light (**d**). Some DNA condensation was observed in cells exposed to ARS-coated TiO<sub>2</sub> nanoparticles (**d**, **h**), and some enlarged nuclei were also observed when ARS-coated TiO<sub>2</sub> nanoparticles were exposed to light (**h**). HeLa cells exposed to dH<sub>2</sub>O (**a**, **e**), ARS (**b**, **f**), and TiO<sub>2</sub> nanoparticles (**c**, **g**) exhibited normal emerin integrity and distribution.

distribution of a second membrane associated protein, lamin B1, was also investigated (Fig. 7). HeLa cells were exposed to the same conditions as in the previous experiment. Alterations in lamin B1 integrity and distribution were detected in HeLa cells exposed to ARS-coated TiO<sub>2</sub> nanoparticles and visible light (Fig. 7h), as nuclear rim staining was decreased and more punctuated when compared to HeLa cells exposed to ARS-coated TiO<sub>2</sub> nanoparticles, but no white light (Fig. 7d). HeLa cells exposed to dH<sub>2</sub>O (Figs. 7a, 7e), ARS (Figs. 7b, 7f), and TiO<sub>2</sub> nanoparticles (Figs. 7c, 7g) demonstrated normal lamin B1 integrity and distribution. Additionally, some cells exposed to ARS-coated TiO<sub>2</sub> nanoparticles and visible light exhibited nuclei with DNA “leaking” outside of the nuclear membrane, and other cells possessed a completely fragmented lamin B1 lamina under these conditions (Fig. 8, white arrows).

## DISCUSSION

Although much advancement has been made in cancer diagnosis and treatment, earlier modes of cancer detection and more specific mechanisms of treatment are still needed to improve the patient prognosis. Biologically and chemically modified TiO<sub>2</sub> nanoparticles have demonstrated much promise in both of these realms due to their ability to be targeted and photoactivated, leading to the localized production of reactive oxygen species (Rajh et al., 2002; Paunesku et al., 2003, 2007, 2008; Thurn et al., 2009, 2011). However, to date TiO<sub>2</sub> nanoparticles have been activated primarily through excitation by UV light (a known mutagen), which limits their use in biological systems (Ashikaga et al., 2000; Long et al., 2006; Park et al., 2008). Recently, fluorescent dyes have been used to coat TiO<sub>2</sub> nanoparticles to enhance their *in*

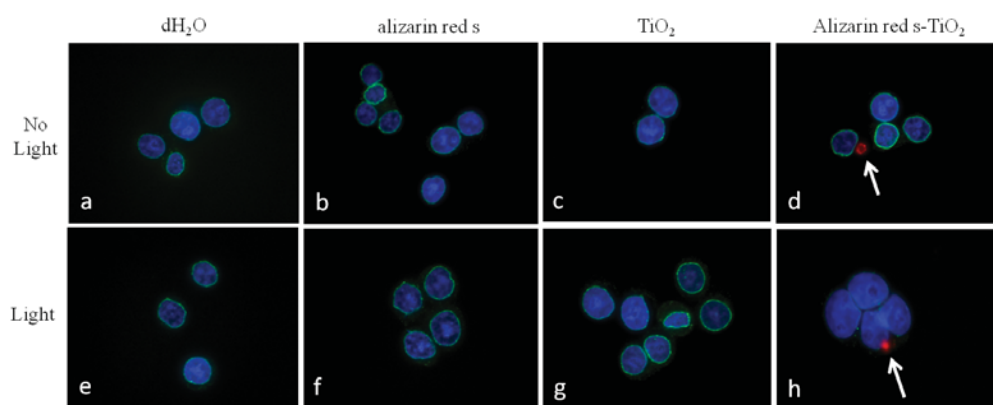


**Figure 7.** Alterations in lamin B1 integrity and distribution were detected in HeLa cells exposed to ARS-coated TiO<sub>2</sub> nanoparticles and white light (h), as nuclear rim staining was decreased and more punctuated, compared to HeLa cells exposed to ARS-coated TiO<sub>2</sub> nanoparticles, but no white light (d). HeLa cells exposed to dH<sub>2</sub>O (a, e), ARS (b, f), and TiO<sub>2</sub> nanoparticles (c, g) exhibited normal emerin integrity and distribution.

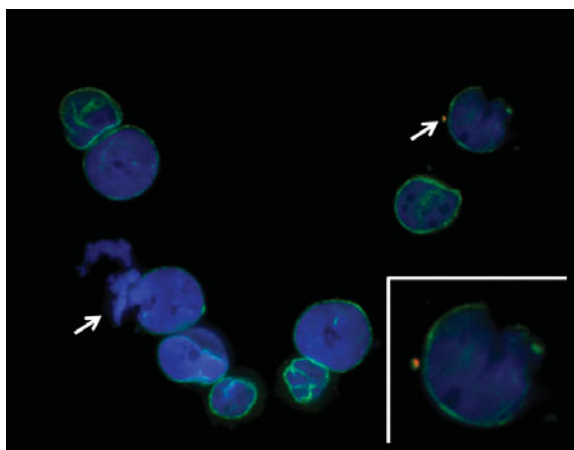


**Figure 8.** Alterations in lamin B1 integrity and distribution were detected in HeLa cells exposed to ARS-coated TiO<sub>2</sub> nanoparticles and white light, as nuclear rim staining was decreased and more punctuated (compared to control cells in Fig. 7). Additionally, some cells exposed to ARS-coated TiO<sub>2</sub> nanoparticles and white light exhibited nuclei with DNA “leaking” outside of the nuclear membrane, and other cells possess fragmented lamin B1 lamina associated with ARS-TiO<sub>2</sub> nanoparticles (white arrows). Inset image is an enlargement of the upper right cell.

*vitro* and *in situ* visualization through fluorescence imaging and microscopy (Brown et al., 2008; Thurn et al., 2009, 2011), and this same coating allows photoactivation of dye-coated TiO<sub>2</sub> nanoparticles through exposure to visible light (Liu et al., 2000). Previous studies have described assays used to study the interactions of ARS with TiO<sub>2</sub> nanoparticles (Rajh et al., 2002; Brown et al., 2008; Thurn et al., 2009).

In the current study, we have added to this dataset by including alterations in fluorescence emission as a study characteristic for assessing dye-TiO<sub>2</sub> interactions, as well as documenting the empirical results obtained for an unsuccessful dye candidate for comparison (Figs. 2, 3). The effects of coating 6 nm TiO<sub>2</sub> nanoparticles with ARS were investigated within the scope of this study, and there is no reason to doubt these findings will extend to different sized TiO<sub>2</sub>

nanoparticles of less than 20 nm in diameter, which have been shown to covalently bond to numerous enediol bidentate ligands (Rajh et al., 2002, 2004; Paunesku et al., 2003, 2007, 2008; Brown et al., 2008; Wu et al., 2008; Thurn et al., 2009, 2011). Our findings are consistent with those investigating related elements, as the binding of ARS to other divalent metal ions such as Zn<sup>2+</sup> and Pb<sup>2+</sup> also results in alteration of fluorescence absorption and emission spectra (Zhang et al., 2007). Herein, we have demonstrated a benefit of visible light activation of dye-coated TiO<sub>2</sub> nanoparticles, which leads to degradation of plasmid DNA through production of reactive oxygen species, while samples containing plasmid DNA in the absence of dye-coated nanoparticles remain unaltered (Figs. 4a, 4b). This same level of plasmid nicking can also be achieved through exposure of dye-coated nanoparticles to UV light; however, at these exposure levels, samples containing solely plasmid DNA also exhibit a moderate level of plasmid nicking (Fig. 4d). Consequently, visible light activation of dye-coated TiO<sub>2</sub> nanoparticles will be of value over UV light activation in applications where protection of neighboring cells and tissues (not containing nanoparticles) is of high importance. These additions will undoubtedly aid in the investigations of future dye coatings of TiO<sub>2</sub> nanoparticles. The perinuclear localization of dye-TiO<sub>2</sub> nanoparticles has been outlined earlier through localization comparisons with the DNA staining dyes in PC-3M cells (Thurn et al., 2009). In the current study, our findings are consistent as we have also documented the perinuclear localization of ARS-coated TiO<sub>2</sub> nanoparticles through 2D and 3D fluorescence confocal studies in reference to two nuclear membrane associated proteins (emerin and lamin B1) in HeLa cells (Fig. 5). By incorporating the study of membrane proteins into our investigation, we also identified that some dye-coated TiO<sub>2</sub> nanoparticles interacted with HeLa cells in a unique manner, creating a donut effect with emerin tunneling through the center of the HeLa cell nucleus and encompassing the ARS nanoconjugates (Fig. 5n, central yellow arrow). This finding will require further investigation but may suggest

that the presence of TiO<sub>2</sub> nanoparticles has an impact upon nuclear integrity independent of photoactivation and/or nuclear membrane reformation following cell division. Moreover, we have also demonstrated that visible light activated ARS-coated TiO<sub>2</sub> nanoparticles are capable of inducing degradation of plasmid DNA *in vitro* and the nuclear membrane of HeLa cells *in situ* through visualizing alterations in the integrity and distribution of these two nuclear membrane associate proteins: emerlin and lamin B1. These findings have implications for live-cell imaging of TiO<sub>2</sub> nanoparticles in cancer cells as well as the development of TiO<sub>2</sub> nanoparticles as a cancer therapy.

It has been shown that visible light irradiation of ARS/TiO<sub>2</sub> dispersions results in generation of active oxygen radicals of superoxide (O<sub>2</sub><sup>•-</sup> or HOO<sup>•</sup>) and hydroxyl radicals (•OH) (Liu et al., 1999, 2000). This supports the findings presented herein illustrating that visible light excited ARS coated-TiO<sub>2</sub> nanoparticles can induce cleavage of plasmid DNA *in vitro* (Fig. 4) and alterations in the integrity and distribution of emerlin and lamin B1 in HeLa cells *in situ* (Figs. 6–8). In addition to producing reactive oxygen species upon photoexcitation, it has been shown that titanium dioxide nanoparticles larger than 2 nm are capable of creating electropositive holes when coated with insulators such as glycidyl isopropyl ether and conjugated to conductive leads (Rajh et al., 2001; Paunesku et al., 2003). Excitation of ARS-coated TiO<sub>2</sub> nanoparticles has been shown to result in ultrafast electron transfer exclusively to localized Ti sites, which is similar to other surface modifiers and results in the accumulation of electropositive holes on ARS, though the exact mechanism is still unknown (Huber et al., 2000; Rajh et al., 2002; Craig et al., 2005). These electropositive holes can interact directly with a biological target or with the aqueous environment to produce reactive oxygen species. Reactive oxygen species only exist for a short time and only travel short distances in solution or cells (Moan, 1990; Niedre et al., 2002; Hall & Giaccia, 2006), so the ability to tether TiO<sub>2</sub> nanoparticles in close spatial proximity to their targets will greatly enhance localized therapeutic efficacy using this approach. These findings, in light of this study, indicate that biologically and chemically modified TiO<sub>2</sub> nanoparticles follow multiple post-excitation events dependent upon design.

Another finding of our study was that exposure of HeLa cells to dye-coated TiO<sub>2</sub> nanoparticles resulted in DNA condensation. This is consistent with the findings of others that showed how photoactivated, bare TiO<sub>2</sub> nanoparticles resulted in DNA condensation in chromatin of epithelial cells (Chen et al., 2008). In our study, we notice DNA condensation in HeLa cells exposed to ARS-coated TiO<sub>2</sub> nanoparticles irrespective of light treatment; however, we only witnessed enlarged nuclei and alterations in integrity and distribution in nuclear membrane associated proteins when samples were exposed to visible light. This suggests either different mechanisms or exposure thresholds in the responses leading to these various phenomena. Some degree of biological variation exists in the responses of HeLa cells to dye-TiO<sub>2</sub> nanoparticles as profound to minimal alter-

ations were detected in our samples, but this is to be expected as the tolerances of individual cells naturally differ. Another notable finding of our study is that some responses are seen in cells that are not directly adjacent to nanoparticles in the field of view. This is not surprising as earlier studies comparing fluorescence microscopy and X-ray fluorescence microscopy techniques for visualization of TiO<sub>2</sub> nanoparticles determined the minimum threshold of ARS-TiO<sub>2</sub> nanoparticles detectable via fluorescence microscopy to be  $7.9 \times 10^4$  (Thurn et al., 2009). So a limitation of our current study is that we are likely not able to visualize all dye-coated TiO<sub>2</sub> nanoparticles that are present in our sample. Despite this limitation, the findings of this study in the context of the existing literature highlight that dye coating of TiO<sub>2</sub> nanoparticles enables activation through exposure to low intensity visible light that inflicts damage on neighboring biological structures both *in vitro* and *in situ*.

## CONCLUSIONS

This study expands upon previous studies that indicated dye coatings on TiO<sub>2</sub> nanoparticles serve to enhance imaging, by clearly showing that dye coatings on TiO<sub>2</sub> nanoparticles can also enhance the photoreactivity of TiO<sub>2</sub> nanoparticles and allow visible light activation. Visible light activation of ARS-TiO<sub>2</sub> nanoparticles results in degradation of biological structures, including DNA cleavage of plasmid DNA *in vitro* and disruption of membrane associated proteins (emerlin and lamin B1) *in situ*. The findings of our study suggest limitations on the use of dye assisted visualization of TiO<sub>2</sub> nanoparticles in live-cell imaging; however, at the same time they may reveal therapeutic applications of dye-coated TiO<sub>2</sub> nanoparticles in cancer research.

## ACKNOWLEDGMENTS

The authors would like to thank the Microscopy Society of America for supporting this work through an Undergraduate Research Scholarship awarded to Jay Blatnik and Eric Brown. Additionally, Jay Blatnik, Lanette Luebke, Megan Nelson, Race Price, Rachael Leek, and Eric Brown would like to thank the College of Letters and Sciences, Office of Research and Sponsored Programs, and Undergraduate Research Program at the University of Wisconsin-Whitewater as well as Wisys for supporting this work through a Faculty Start-Up Grant, Library Research Fellowship, Undergraduate Research Grant, and Applied Research Grant, respectively. Leyong Zeng would like to thank Ningbo Natural Science Foundation of China (Grants No. 2010A610159) and Postdoctoral Science Foundation of China (Grant No. 20100480072) for financial support. Aiguo Wu is appreciative for the support provided by the Zhejiang Provincial Natural Science Foundation of China under Grant No. R5110230, NSFC (Nos. 31170964 and 31128007), the CAS/SAFEA International Partnership Program for Creative Research Teams, the Science and Technology Innovative Research Team of Ningbo Municipality (Grant No. 2009B21005), and the Scientific Research Foundation

for the Returned Overseas Chinese Scholars from State of Ministry of Human Resources & Social Security.

## REFERENCES

- ARSAC, F. & HIDAKA, H. (2007). DNA damage photoinduced by titanium dioxide in the presence of anionic vesicles under UV illumination: Influence of sodium chloride concentration. *J Oleo Sci* **56**(11), 595–601.
- ASHIKAGA, T., WADA, M., KOBAYASHI, H., MORI, M., KATSUMURA, Y., FUKUI, H., KATO, S., YAMAGUCHI, M. & TAKAMATSU, T. (2000). Effect of the photocatalytic activity of TiO<sub>2</sub> on plasmid DNA. *Mutat Res* **466**(1), 1–7.
- BROWN, E.M., PAUNESKU, T., WU, A., THURN, K.T., HALEY, B., CLARK, J., PRIESTER, T. & WOLOSCHAK, G.E. (2008). Methods for assessing DNA hybridization of peptide nucleic acid-titanium dioxide nanoconjugates. *Anal Biochem* **383**(2), 226–235.
- CHEN, E., RUVALCABA, M., ARAUJO, L., CHAPMAN, R. & CHIN, W.C. (2008). Ultrafine titanium dioxide nanoparticles induce cell death in human bronchial epithelial cells. *J Exp Nanosci* **3**(3), 171–183.
- CRAIG, C.F., DUNCAN, W.R. & PREZHDO, O.V. (2005). Trajectory surface hopping in the time-dependent Kohn-Sham approach for electron-nuclear dynamics. *Phys Rev Lett* **95**(16), 163001.
- GOLE, J.L., STOUT, J.D., BURDA, C., LOU, Y.B. & CHEN, X.B. (2004). Highly efficient formation of visible light tunable TiO<sub>2</sub>-xNx photocatalysts and their transformation at the nanoscale. *J Phys Chem B* **108**(4), 1230–1240.
- HALL, E.J. & GIACCIA, A. (2006). Physics and chemistry of radiation absorption. In *Radiobiology for the Radiologist*, Chap. 1, pp. 5–15. Philadelphia, PA: Lippincott Wilkins & Williams.
- HASHIMOTO, K., IRIE, H. & FUJISHIMA, A. (2005). TiO<sub>2</sub> photocatalysis: A historical overview and future prospects. *Japan J Appl Phys* **44**(12), 8269–8285.
- HUBER, R.S., MOSER, J.E., GRATZEL, M. & WACHTVEITL, J. (2000). The role of surface states in the ultrafast photoinduced electron transfer from sensitizing dye molecules to semiconductor colloids. *J Phys Chem B* **104**, 8995–9003.
- LIU, G.L., LI, X., ZHAO, J., HORIKOSHI, S. & HIDAKA, H. (2000). Photooxidation mechanism of dye alizarin red in TiO<sub>2</sub> dispersions under visible illumination: An experimental and theoretical examination. *J Molec Catal A* **153**, 221–229.
- LIU, G., WU, T., ZHAO, J., HIDAKA, H. & SERPONE, N. (1999). Photoassisted degradation of dye pollutants. 8. Irreversible degradation of alizarin red under visible light radiation in air-equilibrated aqueous TiO<sub>2</sub> dispersions. *Environ Sci Technol* **33**(12), 2081–2087.
- LONG, T.C., SALEH, N., TILTON, R.D., LOWRY, G.V. & VERONESI, B. (2006). Titanium dioxide (P25) produces reactive oxygen species in immortalized brain microglia (BV2): Implications for nanoparticle neurotoxicity. *Environ Sci Technol* **40**(14), 4346–4352.
- MICHELMORE, A., GONG, W.Q., JENKINS, P. & RALSTON, J. (2000). The interaction of linear polyphosphates with titanium dioxide surfaces. *Phys Chem Chem Phys* **2**(13), 2985–2992.
- MOAN, J. (1990). On the diffusion length of singlet oxygen in cells and tissue. *Photochem Photobiol B* **6**, 343–347.
- NIEDRE, M., PATTERSON, M.S. & WILSON, B.C. (2002). Direct near-infrared luminescence detection of singlet oxygen generated by photodynamic therapy in cells *in vitro* and tissues *in vivo*. *Photochem Photobiol* **75**, 382–391.
- PARK, E.J., YI, J., CHUNG, K.H., RYU, D.Y., CHOI, J. & PARK, K. (2008). Oxidative stress and apoptosis induced by titanium dioxide nanoparticles in cultured BEAS-2B cells. *Toxicol Lett* **180**(3), 222–229.
- PAUNESKU, T., KE, T., DHARMAKUMAR, R., MASCHERI, N., WU, A., LAI, B., VOGT, S., MASER, J., THURN, K., SZOLC-KOWALSKA, B., LARSON, A., BERGAN, R.C., OMARY, R., LI, D., LU, Z.R. & WOLOSCHAK, G.E. (2008). Gadolinium-conjugated TiO<sub>2</sub>-DNA oligonucleotide nanoconjugates show prolonged intracellular retention period and T1-weighted contrast enhancement in magnetic resonance images. *Nanomedicine* **4**(3), 201–207.
- PAUNESKU, T., RAJH, T., WIEDERRECHT, G., MASER, J., VOGT, S., STOJICEVIC, N., PROTIC, M., LAI, B., ORYHON, J., THURNAUER, M. & WOLOSCHAK, G. (2003). Biology of TiO<sub>2</sub>-oligonucleotide nanocomposites. *Nat Mater* **2**(5), 343–346.
- PAUNESKU, T., VOGT, S., LAI, B., MASER, J., STOJICEVIC, N., THURN, K.T., OSIPO, C., LIU, H., LEGNINI, D., WANG, Z., LEE, C. & WOLOSCHAK, G.E. (2007). Intracellular distribution of TiO<sub>2</sub>-DNA oligonucleotide nanoconjugates directed to nucleolus and mitochondria indicates sequence specificity. *Nano Lett* **7**(3), 596–601.
- RAJH, T., CHEN, L.X., LUKAS, K., LIU, T., THURNAUER, M.C. & TIEDE, D.M. (2002). Surface restructuring of nanoparticles: An efficient route for ligand-metal oxide crosstalk. *J Phys Chem B* **106**(41), 10543–10552.
- RAJH, T., POLUEKTOV, O., DUBINSKI, A.A., WIEDERRECHT, G., THURNAUER, M.C. & TRIFUNAC, A.D. (2001). Spin polarization mechanisms in early stages of photoinduced charge separation in surface-modified TiO<sub>2</sub> nanoparticles. *Chem Phys Lett* **344**(1–2), 31–39.
- RAJH, T., SAPONIJC, Z., LIU, J., DIMITRIJEVIC, N.M., SCHERER, N.F., VEGA-ARROYO, M., ZAPOL, P., CURTISS, L.A. & THURNAUER, M.C. (2004). Charge transfer across the nanocrystalline-DNA interface: Probing DNA recognition. *Nano Lett* **4**(6), 1017–1023.
- SUGDEN, J.K. (2004). Photochemistry of dyes and fluorochromes used in biology and medicine: Some physicochemical background and current applications. *Biotech Histochem* **79**(2), 71–90.
- SUGDEN, K.D., RIGBY, K.M. & MARTIN, B.D. (2004). Oxidative activation of the human carcinogen chromate by arsenite: A model for synergistic metal activation leading to oxidative DNA damage. *Toxicol In Vitro* **18**(6), 741–748.
- THEVENOT, P., CHO, J., WAVHAL, D., TIMMONS, R.B. & TANG, L.P. (2008). Surface chemistry influences cancer killing effect of TiO<sub>2</sub> nanoparticles. *Nanomed-Nanotechnol* **4**(3), 226–236.
- THURN, K.T., ARORA, H., PAUNESKU, T., WU, A., BROWN, E.M., DOTY, C., KREMER, J. & WOLOSCHAK, G. (2011). Endocytosis of titanium dioxide nanoparticles in prostate cancer PC-3M cells. *Nanomedicine* **7**(2), 123–130.
- THURN, K.T., PAUNESKU, T., WU, A., BROWN, E.M.B., LAI, B., VOGT, S., MASER, J., ASLAM, M., DRAVID, V., BERGAN, R. & WOLOSCHAK, G. (2009). Labeling TiO<sub>2</sub> nanoparticles with dyes for optical fluorescence microscopy and determination of TiO<sub>2</sub> DNA nanoconjugate stability. *Small* **5**(11), 1318–1325.
- TSUANG, Y.H., SUN, J.S., HUANG, Y.C., LU, C.H., CHANG, W.H.S. & WANG, C.C. (2008). Studies of photokilling of bacteria using titanium dioxide nanoparticles. *Artif Organs* **32**(2), 167–174.
- WU, A., PAUNESKU, T., BROWN, E.M.B., BABBO, A., CRUZ, C., ASLAM, M., DRAVID, V. & WOLOSCHAK, G.E. (2008). Titanium dioxide nanoparticles assembled by DNA molecules hybridization and loading of DNA interacting proteins. *Nano* **3**(1), 27–36.
- ZHANG, L., DONG, S. & ZHU, L. (2007). Fluorescent dyes of the esculetin and alizarin families respond to zinc ions ratiometrically. *Chem Commun (Camb)* **19**, 1891–1893.